



Minerva Access is the Institutional Repository of The University of Melbourne

Author/s:

Ma, HZ;McKay, AI;Canty, AJ;O'Hair, RAJ

Title:

Using electrospray ionization-tandem mass spectrometry to explore formation and gas-phase chemistry of silver nanoclusters generated from the reaction of silver salts with NaBH₄ in the presence of bis(diphenylarsino)methane

Date:

2021-04-01

Citation:

Ma, H. Z., McKay, A. I., Canty, A. J. & O'Hair, R. A. J. (2021). Using electrospray ionization-tandem mass spectrometry to explore formation and gas-phase chemistry of silver nanoclusters generated from the reaction of silver salts with NaBH₄ in the presence of bis(diphenylarsino)methane. *Journal of Mass Spectrometry*, 56 (4), <https://doi.org/10.1002/jms.4590>.

Persistent Link:

<https://hdl.handle.net/11343/276069>

Submitted to AOMSC 2020 JMS Special Issue

Revised Version: 8 June 2020

Using ESI-MS/MS to explore formation and gas-phase chemistry of silver nanoclusters generated from the reaction of silver salts with NaBH₄ in the presence of bis(diphenylarsino)methane

Howard Z. Ma,^a Alasdair I. McKay,^a Allan J. Canty,^b and Richard A. J. O'Hair^{a*}

(a) School of Chemistry and Bio21 Molecular Science and Biotechnology Institute, University of Melbourne, 30 Flemington Rd, Parkville, Victoria 3010, Australia. Fax: (+) 61 3 9347 8124; E-mail: rohair@unimelb.edu.au

(b) School of Natural Sciences - Chemistry, University of Tasmania, Private Bag 75, Hobart, Tasmania 7001, Australia.

RUNNING TITLE: Gas-phase silver borohydride cluster cations
KEYWORDS: Mass spectrometry, Silver, Cluster, Hydride, Fragmentation, DFT.
This is the author manuscript accepted for publication and has undergone full peer review but has not been through the copyediting, typesetting, pagination and proofreading process, which may lead to differences between this version and the final version. Please refer to this article as doi: [10.1002/jms.4590](https://doi.org/10.1002/jms.4590)

ABSTRACT

Electrospray ionization-mass spectrometry (ESI-MS) of mixtures of AgBF_4 or AgNO_3 with the capping ligand bis(diphenylarsino)methane ($(\text{Ph}_2\text{As})_2\text{CH}_2 = \text{dpam}$) in a solution of acetonitrile revealed the formation of the following cations: $[\text{Ag}(\text{CH}_3\text{CN})(\text{dpam})]^+$, $[\text{Ag}(\text{dpam})_2]^+$, $[\text{Ag}_2(\text{Cl})(\text{dpam})_2]^+$ and $[\text{Ag}_3(\text{Cl})_2(\text{dpam})_3]^+$. Addition of NaBH_4 to these solutions results in the formation of the cluster cations $[\text{Ag}_2(\text{BH}_4)(\text{dpam})_2]^+$, $[\text{Ag}_2(\text{BH}_4)(\text{dpam})_3]^+$, $[\text{Ag}_3(\text{H})(\text{BH}_4)(\text{dpam})_3]^+$, $[\text{Ag}_3(\text{BH}_4)_2(\text{dpam})_3]^+$, $[\text{Ag}_3(\text{H})(\text{Cl})(\text{dpam})_3]^+$ and $[\text{Ag}_3(\text{I})(\text{BH}_4)(\text{dpam})_3]^+$, as established by ESI-MS. Use of NaBD_4 confirmed that borohydride is the source of the hydride in these clusters. An Orbitrap Fusion LUMOS mass spectrometer was used to explore the gas-phase unimolecular chemistry of selected clusters via multistage mass spectrometry (MS^n) experiments employing low-energy collision induced dissociation (CID) and high-energy collision induced dissociation (HCD) experiments. The borohydride containing clusters fragment via two competing pathways: (i) ligand loss; (ii) B-H bond activation involving BH_3 loss.

Density functional theory (DFT) calculations were used to calculate the energetics of the optimized structures for all precursor ions, fragment ions and neutrals and to estimate the reaction endothermicities. Generally there is reasonable agreement between the most abundant product ion formed and the predicted endothermicity of the associated reaction channel. The DFT calculations predicted that the novel dimer $[\text{Ag}_2(\text{BH}_4)(\text{dpam})_2]^+$ has a paddlewheel structure in which the dpam and BH_4^- ligands bridge both silver centers.

INTRODUCTION

Coinage metal hydride nanoclusters continue to attract interest for their roles as catalysts or stoichiometric reagents in synthesis as well as for their novel structural bonding arrangements.¹ For example, Stryker's reagent, $[\text{CuH}(\text{PPh}_3)]_6$, is widely used in stereoselective reductions² and the hydride cluster ions, $[\text{M}_2\text{H}(\text{L})]^+$ ($\text{M} = \text{Cu}, \text{Ag}, \text{Au}$; $\text{L} = \text{bis}(\text{diphenylphosphino})\text{methane}$ (dppm), $\text{bis}(\text{dicyclohexylphosphino})\text{methane}$ (dcpm), 1,8-naphthyridine (napy)), have been shown to selectively extrude CO_2 from formic acid.³⁻⁶ Electrospray ionization-mass spectrometry (ESI-MS) has proven to be a sensitive tool to study the growth of gold nanoclusters⁷⁻¹⁵ and we have used it to direct synthesis of a range of Ag and Cu nanoclusters (Scheme 1).¹⁶⁻²³ The nature of the metal, ligand and reducing agent stoichiometries, solvent and reaction temperature all play crucial roles in the types of clusters that are formed. While the structural motif " $\text{M}_3(\mu_3\text{-H})$ " is common in the trinuclear complexes $[\text{M}_3(\mu_3\text{-H})(\mu_3\text{-BH}_4)(\text{L})_3](\text{BF}_4)$ (where $\text{M} = \text{Ag}$ or Cu , $\text{L} = \text{bis}(\text{diphenylphosphino})\text{methane}$ ($(\text{Ph}_2\text{P})_2\text{CH}_2 = \text{dppm}$ or $\text{bis}(\text{diphenylphosphino})\text{amine} = (\text{Ph}_2\text{P})_2\text{NH} = \text{dppa}$),^{18-19,21} $[\text{Ag}_3(\mu_3\text{-H})(\text{dppm})_3](\text{BF}_4)_2$ and $[\text{Ag}_3(\mu_3\text{-H})(\mu_3\text{-Cl})(\text{dppm})_3](\text{BF}_4)$,¹⁶⁻¹⁷ larger clusters are also observed. In the case of the ligand dppa, the use of copper salts gave rise to the $[\text{Cu}_{16}(\text{H})_{14}(\text{dppa})_6]^{2+}$ dication which was shown via X-ray crystallography to have a core structure consisting of a Cu_9 frustum cupola on top of a Cu_7 distorted hexagonal-shape base. Further, use of the ligand dppe ($\text{bis}(\text{diphenylphosphino})\text{ethane} = (\text{Ph}_2\text{P})_2\text{CH}_2\text{CH}_2$) gave rise to a $[\text{Cu}_{18}(\text{H})_{16}(\text{dppe})_6]^+$ dication under similar synthetic conditions to that used to prepare $[\text{Cu}_{16}(\text{H})_{14}(\text{dppa})_6]^{2+}$.²² In contrast, when silver salts are used, the dications $[\text{Ag}_{10}(\text{H})_8(\text{L})_6]^{2+}$ ($\text{L} = \text{dppm}$ or dppa) are formed and in the case of $[\text{Ag}_{10}(\text{H})_8(\text{dppa})_6](\text{BF}_4)_2$, and $[\text{Ag}_{10}(\text{H})_8(\text{dppa})_6](\text{NO}_3)_2$ these were structurally characterized via X-ray crystallography.²³⁻²⁵ Both dications have nearly identical structural features consisting of a Ag_{10} scaffold with the

atoms lying on vertices of a bicapped square antiprism.²³ Not all clusters are stable over various timeframes. For example, we did not observe $[\text{Ag}_{10}(\text{H})_8(\text{L})_6]^{2+}$ (where L = bis(dimethylphosphino)methane $((\text{Me}_2\text{P})_2\text{CH}_2 = \text{dmpm})$,²⁶ while over time in solution $[\text{Ag}_3(\mu_3\text{-H})(\text{BH}_4)(\text{dppm})_3](\text{BF}_4)$ transformed into the interstitial cluster $[\{\text{Cl}@\text{Ag}_{12}\}@\text{Ag}_{48}(\text{dppm})_{12}]$.²⁷

Scheme 1 Here

The analogous arsine ligand bis(diphenylarsino)methane $((\text{Ph}_2\text{As})_2\text{CH}_2 = \text{dpam})$ has been previously used to prepare the trinuclear silver halide cluster $[\text{Ag}_3(\mu_3\text{-Cl})_2(\text{dpam})_3](\text{Cl})$.²⁸ However, there are no reports on the products from silver salts in the presence of dpam and a reducing agent. Given that the assembly and stability of these clusters appears to depend on both the anionic ligands as well as the bidentate ligand, here we: (i) explore how changing the bidentate ligand to dpam influences the types of nanoclusters formed; (ii) examine the gas-phase unimolecular chemistry of these new nanoclusters; (iii) reveal insights into unique bonding arrangements by Density Functional Theory (DFT) calculations. A rich range of clusters, $[\text{Ag}_2(\text{BH}_4)(\text{dpam})_n]^+$ ($n = 2$ and 3), $[\text{Ag}_3(\text{BH}_4)_2(\text{dpam})_3]^+$ and $[\text{Ag}_3(\text{I})(\text{BH}_4)(\text{dpam})_3]^+$ were characterized, which were not observed when bisphosphine ligands were deployed.

EXPERIMENTAL

Materials and General Methods

The following chemicals were obtained from suppliers and used without further purification: AgBF₄, dpam (Strem); AgNO₃ (Chem-Supply); NaBH₄ (Ajax); NaBD₄ (99 atom % D, Cambridge Isotope Laboratories), acetonitrile (HPLC grade, Burdick & Jackson).

Sample Preparation

AgBF₄ (4 mg, 0.02 mmol) or AgNO₃ (3.5 mg, 0.02 mmol) and bis(diphenylarsino)methane = dpam (10 mg, 0.02 mmol) were dissolved in CH₃CN (5 mL). NaBH₄ or NaBD₄ (8 mg, 0.2 mmol; 9 mg, 0.2 mmol) was then added and allowed to mix for 15 min. An aliquot in CH₃CN, typically 10 μM, was then subsequently taken for MS analyses.

Mass Spectrometry

ESI-MS experiments as well as CID-MSⁿ and HCD-MS/MS multistage mass spectrometry experiments were conducted on an Orbitrap Fusion LUMOS (Thermo Fisher Scientific, San Jose, California). Samples were introduced into the mass spectrometer as 10 μM solutions via a heated electrospray ionization (HESI) source at an injection rate of 5 μL min⁻¹. Typical source conditions were as follows; spray voltage of 3.6 kV, heated capillary temperature of 250 °C, sheath gas pressure of 5 – 20 psi, aux gas flow of 2.5 a.u., sweep gas flow of 5 – 10 a.u. and vaporizer temperature of 20 °C, with the RF lens set to 60 – 80 %. ESI-MS spectra to survey the formation of cluster ions formed were typically acquired from m/z 200 – 2000 to observe the full range of products formed before acquiring from m/z 500 – 2000 to focus on the cluster ions of interest. Spectra were acquired at a mass resolving power of 500,000 and an AGC target of 5.0×10^5 . For CID-MSⁿ and HCD-MS/MS experiments, mass selection was carried out using the isolation quadrupole ($\pm 0.2 - 0.5 m/z$) on the mono-isotopic precursor ions where possible or the most abundant ion of the full isotopic envelope, see Fig. S1-S2 for example. For CID-MSⁿ, the mass selected precursor ion was then subjected to ion trap CID using an activation Q of 0.25 and

an activation time of 10 ms. For HCD-MS/MS, the mass selected precursor ion was subjected to the collision cell where collision energies were individually optimized for fragment ion efficiency. Spectra shown are the average of 25 – 100 scans in order to provide appropriate signal-to-noise ratios. Preliminary experiments were carried out on a Finnigan LTQ linear ion trap mass spectrometer (Bremen, Germany).

Theoretical calculations

Geometry optimizations were performed with the Perdew-Burke-Ernzerhof (PBE) functional^{29,30} with resolution of identity method (W06)^{31,32} and relativistic effective core potential (RECP) basis set^{33,34} for silver and iodine atoms in combination with the split-valence-plus polarization (SVP) atomic basis set^{35,36} for all other atoms with Grimme's D3 dispersion correction³⁷ using the Gaussian 16 suite of programs.³⁸ PBE analytical harmonic vibrational frequency calculations validated reactants and products as energy minima.

For all geometries optimized at the RI-PBE/RECP-def2-SVP level of theory, single-point energies were calculated with the range-separated meta-GGA hybrid density functional ω B97M-V with D3BJ.^{37,39-41} In order to compare the merits of various density functionals, single-point energies were also calculated with the meta-GGA B97M-D3BJ^{37,40-42} and hybrid meta-GGA MN15 density functionals.^{43,44} The density functionals, MN15, B97M-V and ω B97M-V, considered for the single-point energy calculations were based upon a recent study by Chan et al. that looked at and assessed several DFT methods and their accuracies for transition metal systems.⁴⁵ Overall, the best performing DFT methods were MN15, B97M-V and ω B97M-V. A comparison of the three density functionals is summarized in the Supporting Information (Tables

S4-8). For ω B97M-V and B97M-V calculations, the def2-TZVP basis set was used for main group atoms³¹ with an effective core potential for Ag and I atoms.^{33,34} For MN15 calculations, the def2-TZVP basis set³¹ was also used and, where appropriate, associated effective core potentials were used for Ag and I atoms. Single point energy calculations using the ω B97M-V and B97M-V density functionals were performed with ORCA 4.2.0⁴⁶⁻⁴⁸ and Gaussian 16 was used for MN15 calculations.³⁸ To estimate the corresponding enthalpy, ΔH , and Gibbs free energies, ΔG , the corrections were calculated at the RI-PBE level of theory and finally added to the corresponding single-point energies. The corrected ΔG and ΔH values calculated at the ω B97M-D3BJ/def2-TZVP level of theory have been used throughout unless stated otherwise.

RESULTS AND DISCUSSION

ESI-MS survey of the formation of silver nanocluster cations with bis(diphenylarsino)methane and NaBH_4

ESI-MS of a 1:1 mixture of the silver salt AgBF_4 and bis(diphenylarsino)methane in CH_3CN yields mono-, bi-, and tri-nuclear nanoclusters (Figs. 1a and S3). A common feature of the types of clusters formed is the incorporation of halides including the tri-nuclear dichloride cluster $[\text{Ag}_3(\text{Cl})_2(\text{dpam})_3]^+$ (m/z 1810) which has been previously structurally characterized by X-ray crystallography by Skelton, White and co-workers.²⁸ The analogous dihalide cluster ions are also observed, $[\text{Ag}_3(\text{I})(\text{Cl})(\text{dpam})_3]^+$ (m/z 1903) and $[\text{Ag}_3(\text{I})_2(\text{dpam})_3]^+$ (m/z 1995) (Fig. S4). While the source of the halides in these clusters is unclear, the high affinity of silver for halides suggests that even minor halide impurities are readily intercepted, as noted in a previous study.²⁶ Other prominent cations observed include $[\text{Ag}(\text{CH}_3\text{CN})(\text{dpam})]^+$ (m/z 620), $[\text{Ag}(\text{dpam})_2]^+$ (m/z 1053)

and $[\text{Ag}_2(\text{Cl})(\text{dpam})_2]^+$ (m/z 1195). The related ions have been previously reported for dppm ¹⁷ and dmpm .²⁶ The bulkier phosphine ligand dppm tends to stabilize di-nuclear species, e.g. $[\text{Ag}_2(\text{dppm})_2]^{2+}$, whereas the smaller phosphine ligand dmpm and bulky arsine ligand dpam are able to stabilize a larger range of clusters (Table S1).

Figure 1 Here

Upon addition of a 10-fold excess of NaBH_4 to the 1:1 mixture of silver salt and bis(diphenylarsino)methane in CH_3CN , there is a notable color change in the reaction mixture from colorless to orange, which upon electrospray ionization of the sample shows a significant change in the product ions observed in the ESI-MS spectrum (Fig. 1b). Notably, several borohydride (BH_4^-) containing clusters are formed including $[\text{Ag}_2(\text{BH}_4)(\text{dpam})_2]^+$ (m/z 1175), $[\text{Ag}_2(\text{BH}_4)(\text{dpam})_3]^+$ (m/z 1646), $[\text{Ag}_3(\text{H})(\text{BH}_4)(\text{dpam})_3]^+$ (m/z 1756) and $[\text{Ag}_3(\text{BH}_4)_2(\text{dpam})_3]^+$ (m/z 1768). The mixed hydride/borohydride species is the direct arsenic cluster ion equivalent of the $[\text{Ag}_3(\mu_3\text{-H})(\mu_3\text{-BH}_4)(\text{L})_3](\text{BF}_4)$, $\text{L} = \text{dppm}$ and dppa , trinuclear silver nanocluster previously synthesized and fully characterized via X-ray crystallography, multinuclear NMR spectroscopy and FTIR spectroscopy.^{18,21} The other BH_4^- containing ions however were not previously observed where $\text{L} = \text{dppm}$, dppa or dmpm and represent new cluster species for which their unimolecular gas-phase chemistry was investigated and is described below.

Table S2 compares the types of nanoclusters formed upon NaBH_4 reduction between the three methylene bridged bidentate ligands, where $\text{L} = \text{dppm}$, dpam and dmpm . Notably, the decasilver(I) octahydride dicationic cluster $[\text{Ag}_{10}(\text{H})_8(\text{L})_6]^{2+}$ is only observed when dppm is employed,²³⁻²⁵ neither the arsenic equivalent (dpam) nor the less sterically bulky equivalent

(dmpm)²⁶ are able to produce the larger homometallic silver hydride nanocluster. Further, the amine equivalent dppa is also able to produce the decanuclear Ag₁₀ species which we were recently able to isolate and structurally characterize via X-ray crystallography and other methods.²³ These observations suggest that both the steric bulk provided by the phenyl groups, and the binding strength of the ligand play a role in the stabilization of larger clusters and more importantly the nature of the types of nanoclusters formed. Finally, the BH₄⁻ containing clusters as mentioned above are entirely unique to the arsine ligand (dpam).

Table 1 Here

To better understand why these clusters are unique to dpam and to suggest why the larger [Ag₁₀(H)₈(dpam)₆]²⁺ dication is unable to be formed, we have investigated the relevant bond lengths of several [Ag₃(X)₂(L)₃]⁺ (X = coordinating anionic ligand) cluster frameworks via their known crystal structures (Table 1). Comparing the Ag-P bonds of [Ag₃(H)(BH₄)(dppm)₃]⁺, [Ag₃(H)(Cl)(dppm)₃]⁺ and [Ag₃(Cl)₂(dppm)₃]⁺, we find that the bond lengths are consistent around 2.4 Å regardless of the anions that cap the two faces of the triangle formed by the trinuclear Ag core. Contrastingly, in [Ag₃(Cl)₂(dpam)₃]⁺, the analogous Ag-As bond is consistently longer at an average of 2.5 Å. This suggests that a slightly weaker metal-ligand bond, when switching from dppm to dpam, may play a role in the overall stability of the Ag₁₀ core. This is consistent with DFT studies which have shown a weakening of the [Ag-EH₃]⁺ bond strength when going down the group from nitrogen (E = N) to arsenic (E = As).⁴⁹ Further, ESI-MS studies on the relative ligand properties of the triphenylpnictogen ligands EPh₃ (E = P, As, Sb and Bi) towards silver(I) ions found that the preferred species formed increase in coordination

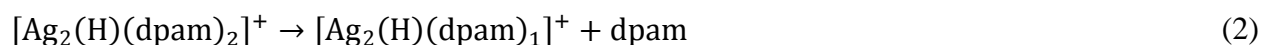
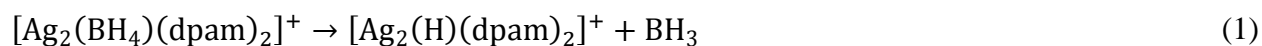
number from two for PPh_3 in $[\text{Ag}(\text{PPh}_3)_2]^+$ to four for SbPh_3 in $[\text{Ag}(\text{SbPh}_3)_4]^+$, consistent with the decreasing donor ligand ability in the series PPh_3 , AsPh_3 and SbPh_3 .⁵⁰ The Ag-Ag distances appear to be primarily influenced by the nature of the capping anionic ligand rather than the identity of the bidentate ligand. For example, where the cluster contains a single chloride, Ag-Ag distances are around 2.9 Å, in the selected examples, whereas where the cluster contains two chlorides, the distance is significantly longer at around 3.4 Å. This is further highlighted in the related bond distances in the dibromo and diiodo clusters $[\text{Ag}_3(\text{Br})_2(\text{dppm})_3]^+$ and $[\text{Ag}_3(\text{I})_2(\text{dppm})_3]^+$ where the Ag-Ag average bond lengths are around 3.3 Å and 3.2 Å, respectively (Table S3).

Gas-phase unimolecular chemistry of $[\text{Ag}_2(\text{BH}_4)(\text{dpam})_2]^+$, $[\text{Ag}_2(\text{BH}_4)(\text{dpam})_3]^+$, $[\text{Ag}_3(\text{H})(\text{BH}_4)(\text{dpam})_3]^+$ and $[\text{Ag}_3(\text{BH}_4)_2(\text{dpam})_3]^+$.

Previous work has established the gas-phase fragmentation chemistry of the mixed hydride/borohydride trinuclear $[\text{Ag}_3(\text{H})(\text{BH}_4)(\text{dppm})_3]^+$ and $[\text{Ag}_3(\text{H})(\text{BH}_4)(\text{dmpm})_3]^+$ cations.^{18,26} The main fragmentation pathway from the precursor ions $[\text{Ag}_3(\text{H})(\text{BH}_4)(\text{dppm})_3]^+$ and $[\text{Ag}_3(\text{H})(\text{BH}_4)(\text{dmpm})_3]^+$ involves neutral ligand losses to yield $[\text{Ag}_3(\text{H})(\text{BH}_4)(\text{L})_2]^+$ as the primary product ion. Here, we were interested in characterizing the fragmentation chemistry of the novel BH_4^- containing cluster ions $[\text{Ag}_2(\text{BH}_4)(\text{dpam})_2]^+$, $[\text{Ag}_2(\text{BH}_4)(\text{dpam})_3]^+$ and $[\text{Ag}_3(\text{BH}_4)_2(\text{dpam})_3]^+$ by carrying out single-isotope MS^n experiments. The $[\text{Ag}_3(\text{H})(\text{BH}_4)(\text{dpam})_3]^+$ cation is also investigated and compared to its phosphine counterparts.

Figure 2 Here

Mass selection and subsequent low energy CID of $[\text{Ag}_2(\text{BH}_4)(\text{dpam})_2]^+$ (m/z 1174.8795) leads to the formation of $[\text{Ag}_2(\text{H})(\text{dpam})_2]^+$ (m/z 1160.8470) via neutral borane ($^{11}\text{BH}_3$) loss as the main fragmentation pathway (eq. 1, Fig. 2a). Isolation of $[\text{Ag}_2(\text{H})(\text{dpam})_2]^+$ followed by another stage of CID led to neutral ligand loss to give $[\text{Ag}_2(\text{H})(\text{dpam})_1]^+$ (m/z 688.8324) as the major product ion (eq. 2, Fig. 2b). $[\text{Ag}(\text{dpam})_2]^+$ (m/z 1052.9343), via AgH loss, and $[\text{Ag}(\text{dpam})_1]^+$ (m/z 580.9195), likely formed via AgH loss from $[\text{Ag}_2(\text{H})(\text{dpam})_1]^+$, cations are also observed. To further corroborate our assignments of neutral BH_3 loss followed by neutral ligand loss, we have carried out a deuterium labeled study using NaBD_4 as the reagent, thus allowing the “counting” of the number of hydrides by observing the differences in mass shifts. Similar to $[\text{Ag}_2(\text{BH}_4)(\text{dpam})_2]^+$, $[\text{Ag}_2(\text{BD}_4)(\text{dpam})_2]^+$ (m/z 1175.8950) was mass selected and subjected to CID giving $[\text{Ag}_2(\text{D})(\text{dpam})_2]^+$ (m/z 1159.8520) as the major product ion (Fig. S5a). A mass difference of 16 m/z units is indicative of $^{10}\text{BD}_3$ loss from the precursor ion. Under HCD conditions, similar fragmentation channels are observed (Fig. S6-7).



The bulkier tri-ligated $[\text{Ag}_2(\text{BH}_4)(\text{dpam})_3]^+$ (m/z 1643.8990) cation undergoes neutral ligand loss to give $[\text{Ag}_2(\text{BH}_4)(\text{dpam})_2]^+$ (m/z 1171.8839) as the primary product (eq. 3, Fig. 3a). In a second stage of CID, $[\text{Ag}_2(\text{BH}_4)(\text{dpam})_2]^+$ undergoes $^{10}\text{BH}_3$ loss to give $[\text{Ag}_2(\text{H})(\text{dpam})_2]^+$ (m/z 1158.8473) (eq. 1, Fig. 3b) which is identical to the fragmentation of the precursor $[\text{Ag}_2(\text{BH}_4)(\text{dpam})_2]^+$ ion discussed above. Similarly, the deuterated analogue, $[\text{Ag}_2(\text{BD}_4)(\text{dpam})_3]^+$ (m/z 1647.9107), gives a major peak at 1175.8969 m/z which can be

assigned as $[\text{Ag}_2(\text{BD}_4)(\text{dpam})_2]^+$ indicating ligand loss (Fig. S8a), followed by $^{10}\text{BD}_3$ loss to give $[\text{Ag}_2(\text{D})(\text{dpam})_2]^+$ at 1159.8520 m/z (Fig. S8b). HCD-MS/MS of both proteo- and deuterio-species suggest similar fragmentation pathways (Figs. S9-10).

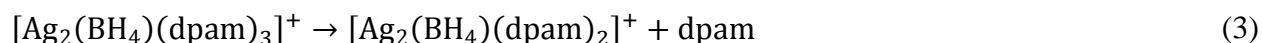


Figure 3 Here

The mixed hydride/borohydride cation $[\text{Ag}_3(\text{H})(\text{BH}_4)(\text{dpam})_3]^+$ (m/z 1754.8080) fragments in a similar manner to its dpmm and dmpm equivalents. First, neutral ligand loss occurs to form $[\text{Ag}_3(\text{H})(\text{BH}_4)(\text{dpam})_2]^+$ (m/z 1282.7934) (eq. 4, Fig. 4a). Previous energy-resolved CID (ERCID) experiments with the phosphine ligands dpmm and dmpm have shown that other ions aside from ligand loss are from subsequent secondary fragmentation channels.¹⁷ Subsequent isolation and CID of $[\text{Ag}_3(\text{H})(\text{BH}_4)(\text{dpam})_2]^+$ reveals a greater variety of product ions in the MS³ spectrum (Fig. 4b). $[\text{Ag}_3(\text{H})_2(\text{dpam})_1]^+$ (m/z 796.7453) appears as the major product ion while $[\text{Ag}_3(\text{H})_2(\text{dpam})_2]^+$ (m/z 1268.7605) and $[\text{Ag}_3(\text{H})(\text{BH}_4)(\text{dpam})_1]^+$ (m/z 810.7783) cations are also observed.

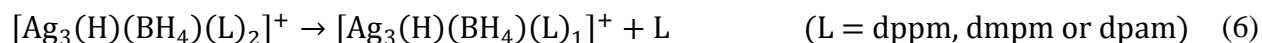
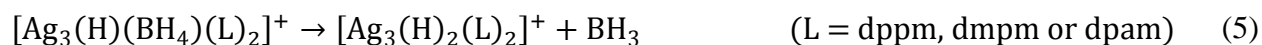
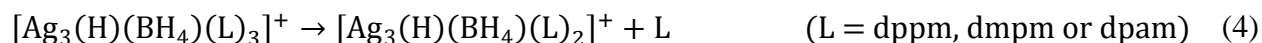


Figure 4 Here

$[\text{Ag}_3(\text{H})_2(\text{dpam})_2]^+$ is formed as a result of BH_3 loss from $[\text{Ag}_3(\text{H})(\text{BH}_4)(\text{dpam})_2]^+$ (eq. 5). $[\text{Ag}_3(\text{H})(\text{BH}_4)(\text{dpam})_1]^+$ is formed via neutral ligand loss (eq. 6). The formation of $[\text{Ag}_3(\text{H})_2(\text{dpam})_1]^+$ is either through neutral ligand loss from $[\text{Ag}_3(\text{H})_2(\text{dpam})_2]^+$ (eq. 7, Fig. S11a) or BH_3 loss from $[\text{Ag}_3(\text{H})(\text{BH}_4)(\text{dpam})_1]^+$ (eq. 8, Fig. S11b) as indicated by CID-MS⁴ spectra. Deuterated $[\text{Ag}_3(\text{D})(\text{BD}_4)(\text{dpam})_3]^+$ undergoes similar fragmentation pathways to its proteo-analogue (Fig. S12) as do HCD-MS/MS spectra (Fig. S13-14).

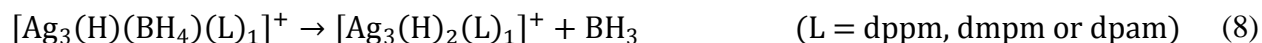
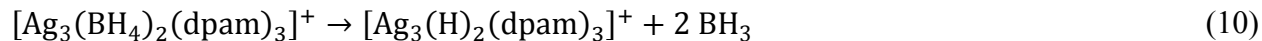
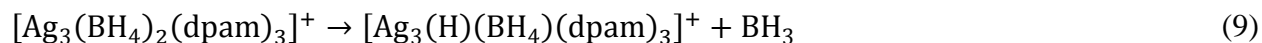


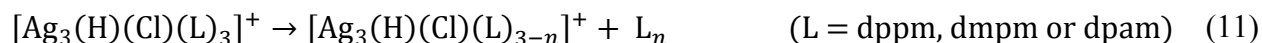
Figure 5 Here

The bis borohydride cluster ion $[\text{Ag}_3(\text{BH}_4)_2(\text{dpam})_3]^+$ initially undergoes BH_3 loss to give the mixed hydride/borohydride species $[\text{Ag}_3(\text{H})(\text{BH}_4)(\text{dpam})_3]^+$ (m/z 1756.8091) (eq. 9). BH_3 loss triggers ligand loss to give $[\text{Ag}_3(\text{H})(\text{BH}_4)(\text{dpam})_2]^+$ (m/z 1284.7932) (eq. 4, Fig. 5a and S15a). The loss of two BH_3 molecules prior to ligand loss, i.e., $[\text{Ag}_3(\text{H})_2(\text{dpam})_3]^+$, is not observed (eq. 10). HCD-MS/MS experiments at lower collision energies provides strong evidence that BH_3 loss proceeds prior to ligand loss (Fig. S16-17).



Gas-phase unimolecular chemistry of $[\text{Ag}_3(\text{H})(\text{Cl})(\text{dpam})_3]^+$ and $[\text{Ag}_3(\text{I})(\text{BH}_4)(\text{dpam})_3]^+$

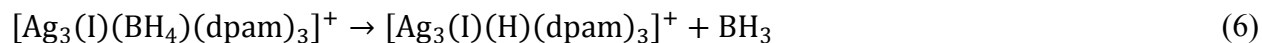
As noted above, while the source of halides in the clusters $[\text{Ag}_3(\text{H})(\text{Cl})(\text{dpam})_3]^+$ and $[\text{Ag}_3(\text{I})(\text{BH}_4)(\text{dpam})_3]^+$ is likely due to trace impurities, the presence of the cluster cations in the ESI-MS offers the opportunity to explore how a coordinated halide influences fragmentation. The unimolecular chemistry of the mixed hydride/chloride cluster $[\text{Ag}_3(\text{H})(\text{Cl})(\text{L})_3]^+$ has been explored for both the dpmm and dmpm variants.^{16,26} Here we find that sequential ligand loss (eq. 11) is the dominant channel as illustrated in Fig. S18. The reductive elimination product $[\text{Ag}_3(\text{L})_3]^+$ is not observed (eq. 12).



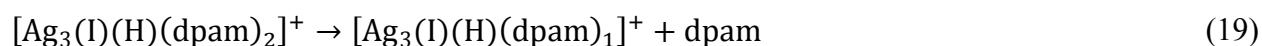
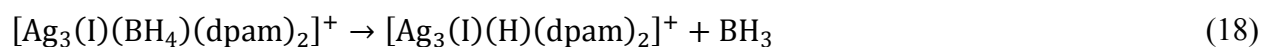
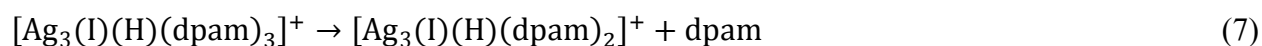
AgH and AgCl losses from $[\text{Ag}_3(\text{H})(\text{Cl})(\text{dpam})_1]^+$ to form $[\text{Ag}_2(\text{Cl})(\text{dpam})_1]^+$ (m/z 722.7926) and $[\text{Ag}_2(\text{H})(\text{dpam})_1]^+$ (m/z 688.8316), respectively, are observed at higher energies via HCD-MS/MS (eq. 13,14, Fig. S19).



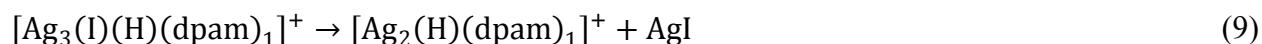
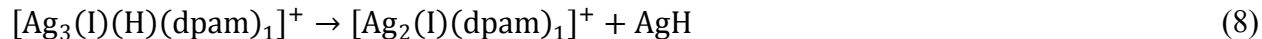
The mixed iodide/borohydride species, $[\text{Ag}_3(\text{I})(\text{BH}_4)(\text{dpam})_3]^+$ (m/z 1882.7604), represents a cluster of new stoichiometry. Under CID conditions, it undergoes ligand loss (eq. 15) with a minor fragmentation channel being neutral BH_3 loss (eq. 16) (Fig. S20-21).



Isolation of $[\text{Ag}_3(\text{I})(\text{H})(\text{dpam})_3]^+$ (m/z 1868.6728) followed by further CID results in ligand loss (eq. 17, Fig. S22a) Initial loss of ligand from the precursor ion to give $[\text{Ag}_3(\text{I})(\text{BH}_4)(\text{dpam})_2]^+$ (m/z 1410.6905) likely triggers the loss of BH_3 (eq. 18). Indeed, isolation of $[\text{Ag}_3(\text{I})(\text{BH}_4)(\text{dpam})_2]^+$ and subjecting the ion to further CID results in the formation of $[\text{Ag}_3(\text{I})(\text{H})(\text{dpam})_2]^+$ (m/z 1396.6573) (Fig. S22b). Lastly, isolation of the mixed iodide/hydride $[\text{Ag}_3(\text{I})(\text{H})(\text{dpam})_2]^+$ leads to further ligand loss giving $[\text{Ag}_3(\text{I})(\text{H})(\text{dpam})_1]^+$ (m/z 924.6422) (eq. 19, Fig. S22c).



Further loss of a ligand from $[\text{Ag}_3(\text{I})(\text{H})(\text{dpam})_2]^+$ is the most likely channel to give $[\text{Ag}_3(\text{I})(\text{H})(\text{dpam})_1]^+$ (m/z 924.6426) as indicated by the HCD-MS/MS spectrum (Fig. S23-24). From the singly ligated cluster ion, silver hydride (AgH) and silver iodide (AgI) extrusion pathways are available to give $[\text{Ag}_2(\text{I})(\text{dpam})_1]^+$ (m/z 814.7300) and $[\text{Ag}_2(\text{H})(\text{dpam})_1]^+$ (m/z 688.8332), respectively (eq. 20,21).



Theoretical calculations exploring the product ion structures and energetics associated with BH_3 and ligand loss

We have previously explored the process of BH_4^- decomposition triggered via ligand loss from the clusters $[\text{Ag}_3(\text{H})(\text{BH}_4)(\text{dmpm})_n]^+$ ($n = 1-3$) whereby the phenyl groups of the dppm ligand were replaced by methyl groups for computational expediency. Here, DFT calculations were carried out with the phenyl groups included in the geometry optimization calculations in order to account for relevant dispersion effects. The gas-phase structure (Fig. 6) and reactivity of the following cations were explored computationally: $[\text{Ag}_2(\text{BH}_4)(\text{dpam})_2]^+$, $[\text{Ag}_3(\text{H})(\text{BH}_4)(\text{dpam})_3]^+$, $[\text{Ag}_3(\text{BH}_4)_2(\text{dpam})_3]^+$, $[\text{Ag}_3(\text{H})(\text{Cl})(\text{dpam})_3]^+$ and $[\text{Ag}_3(\text{I})(\text{BH}_4)(\text{dpam})_3]^+$. For the fragmentation reactions of the clusters, the temperature at which fragmentation occurs is unknown and so we calculate both ΔG and ΔH at 298 K to estimate the energetics associated with competing reaction channels.

Revised Figure 6 Here

Modeling the structure of the BH_4^- coordinated Ag_2 dimer represents a theoretical challenge due to the limited structural evidence for its existence in the literature. However, we have based its structure upon a not too dissimilar cluster $[\text{Ag}_2(\text{BF}_4)(\text{L})_2]^+$ ($\text{L} = (\text{PPh}_2)_2\text{N}(p\text{-OMe})\text{C}_6\text{H}_4$) for

which a crystal structure has been determined.⁵¹ On replacing the dppa-type ligand with dpam and BF_4^- with BH_4^- , reoptimization suggests that the BH_4^- coordinates as a $\mu_2:\kappa^2$ ligand via two hydrides (Fig. 6a). A crystal structure has also been reported for a related neutral binuclear copper(I) complex, $[\text{Cu}_2(\text{BH}_4)_2(\text{dppm})_2]$, which contains two coordinated borohydride ligands.⁵² The structure highlights a $\kappa^2\text{-BH}_4$ coordination mode to the copper(I) centers. By taking the coordinates from the crystal structure, replacing the copper(I) centers with silver(I) centers and the dppm ligand with the corresponding dpam ligand, we have modeled the structure of $[\text{Ag}_2(\text{BH}_4)_2(\text{dpam})_2]$ (Fig. S25). Our modeled structure agrees with the reported crystal structure for the copper(I) complex where the BH_4^- anions bind in a κ^2 geometry. Upon taking this structure and removing either of the two single BH_4^- coordinated ligands, we have reoptimized both resultant mono-cationic complexes $[\text{Ag}_2(\text{BH}_4)(\text{dpam})_2]^+$. We found that the remaining BH_4^- changes its binding mode from κ^2 to $\mu_2:\kappa^2$ as a bridging ligand across the two silver(I) centers (Fig. S26). Although the resultant structures are very similar to that found in Fig. 6a, they are isomers arising from differences in the conformations of the dpam ligands, which highlights the likely fluxional nature of these clusters (Fig. S26). A notable finding is that the BH_4^- ligand exerts a key influence bridging two metal centers rather than coordinate to a single metal center. We have further considered an additional isomer (Isomer 2) for the Ag_2 dimer, $[\text{Ag}_2(\text{BH}_4)(\text{dpam})_2]^+$, whereby the BH_4^- acts as a $\kappa^2:\kappa^2$ -bridging ligand (Fig 6b). This mode of BH_4^- has been observed in structurally characterized monocationic dimers of Fe, Cu and Pd.⁵³⁻⁵⁵ Computations suggest formation of this isomer relative to Isomer 1 to be energetically less favorable by 11.2 kcal/mol, as such we have only considered the ‘paddle-wheel’ structure of Isomer 1 for $[\text{Ag}_2(\text{BH}_4)(\text{dpam})_2]^+$ in all subsequent discussions.

The structures of $[\text{Ag}_3(\text{H})(\text{BH}_4)(\text{dpam})_3]^+$, and $[\text{Ag}_3(\text{H})(\text{Cl})(\text{dpam})_3]^+$ cations were based on existing X-ray crystal structures of $[\text{Ag}_3(\text{H})(\text{BH}_4)(\text{dppm})_3]^+$ and $[\text{Ag}_3(\text{H})(\text{Cl})(\text{dppm})_3]^+$.^{16,18} In each case the phosphine ligands were replaced by arsine ligands and then re-optimized. The structures of $[\text{Ag}_3(\text{BH}_4)_2(\text{dpam})_3]^+$ and $[\text{Ag}_3(\text{I})(\text{BH}_4)(\text{dpam})_3]^+$ were modeled based on the $[\text{Ag}_3(\text{X})_2(\text{L})_3]^+$ framework (Fig. 6) which has been shown to be a common structural motif in coinage metal clusters with a $[\text{M}_3(\text{L})_3]^+$ stoichiometry. In the case of $[\text{Ag}_3(\text{BH}_4)_2(\text{dpam})_2]^+$, DFT methods suggest that the anionic BH_4^- ligands coordinate to the triangular Ag_3 core as two μ_2 ligands via a single hydride from each BH_4^- ligand. This contrasts to the mixed hydride/borohydride $[\text{Ag}_3(\text{H})(\text{BH}_4)(\text{dpam})_3]^+$ in which the BH_4^- ion coordinates as a $\mu_3:\kappa^3$ ligand via three hydrides (Fig. 6c). For $[\text{Ag}_3(\text{I})(\text{BH}_4)(\text{dpam})_3]^+$, both anionic ligands coordinate to the Ag_3 framework as μ_2 ligands bridging two silver(I) centers of the triangular Ag_3 core (Fig. 6f). The diversity of binding modes of BH_4^- ligands in metal complexes has been previously noted.^{56,57}

Figure 7 Here

Fragmentation of the BH_4^- ligand to liberate neutral borane (BH_3) was found to be the dominant fragmentation channel from $[\text{Ag}_2(\text{BH}_4)(\text{dpam})_2]^+$ in the gas-phase unimolecular experiments (eq. 1, Fig. 2a), in comparison to ligand loss which was a minor pathway. Scans were performed for stretching the B-H bond and Ag-As bonds, but no transition states were found. Both ΔG and ΔH (kcal/mol) values suggest that BH_3 loss is the energetically more favorable pathway ($\Delta G = 23.8$

kcal/mol), compared to ligand loss ($\Delta G = 27.1$ kcal/mol) (Fig. 7, Table 2), consistent with the experimental results. For a more detailed summary of the relevant energies, see Tables S4-8.

Table 2 Here

The gas-phase unimolecular chemistry suggests that the mixed hydride/borohydride cluster $[\text{Ag}_3(\text{H})(\text{BH}_4)(\text{dpam})_3]^+$ prefers neutral ligand loss over BH_3 loss (eq. 4, Fig. 4a). Comparisons of the experiments with the calculated energy diagram (Table 2, Fig. S27) reveals agreement with ΔG (kcal/mol) values but not with ΔH (kcal/mol) values, suggesting that entropic factors are important in these fragmentation reactions.

Fig. S28 shows the relevant energetics between competing BH_3 and ligand loss in the novel bis-borohydride $[\text{Ag}_3(\text{BH}_4)_2(\text{dpam})_3]^+$ cation. Here, both ΔG and ΔH predict BH_3 loss as the preferred pathway (Table 2). Indeed, this reflects experimental results which show that BH_3 loss is the initial product ion formed upon MS^n experiments to give $[\text{Ag}_3(\text{H})(\text{BH}_4)(\text{dpam})_3]^+$ (eq. 9, Fig. 5a and S15-17).

In the case of the mixed hydride/chloride cluster $[\text{Ag}_3(\text{H})(\text{Cl})(\text{dpam})_3]^+$, experimental results showed that ligand loss was the only product ion observed, $[\text{Ag}_3(\text{H})(\text{Cl})(\text{dpam})_2]^+$ (eq. 11, Fig. S18-19). The product that would be formed upon reductive elimination, $[\text{Ag}_3(\text{dpam})_3]^+$, via HCl extrusion is not observed (eq. 12). Single-point energy calculations at the $\omega\text{B97M-D3BJ}/\text{def2-TZVP}$ level of theory are in agreement with experimental results (Fig. S29). However, at the B97M-D3BJ and MN15 levels of theory, the opposite trend is predicted, i.e., the reductive

elimination product $[\text{Ag}_3(\text{dpam})_3]^+$, is the more energetically stable product (Table S7). We should note that there is likely to be a higher energy barrier associated with the transition state for reductive elimination (not located) in order for it to proceed experimentally.

Finally, DFT calculations on the mixed iodide/borohydride cluster, $[\text{Ag}_3(\text{I})(\text{BH}_4)(\text{dpam})_3]^+$, suggest BH_3 loss as the preferred pathway in both ΔG and ΔH values (Table 2, Fig. S30). In comparison to our gas-phase experiments, both BH_3 and ligand loss pathways were observed in the MS^2 spectrum of $[\text{Ag}_3(\text{I})(\text{BH}_4)(\text{dpam})_3]^+$ (eq. 17,18, Fig. S20). These theoretically calculated energetics suggest that BH_3 loss is an immediate, facile process from the precursor ion which then triggers subsequent ligand loss. Thus only a small intensity ion is observed for $[\text{Ag}_3(\text{I})(\text{H})(\text{dpam})_3]^+$ (the product ion from BH_3 loss), yet the major product ion observed in the spectrum is $[\text{Ag}_3(\text{I})(\text{H})(\text{dpam})_2]^+$.

CONCLUSIONS

Short bite angle ligands such as dppm and dpam have a rich history in transition metal cluster chemistry. While there are examples where the substitution of dpam for dppm results in clusters of the same stoichiometry and possessing similar structures,⁵⁸ much less is known for silver clusters. Here we have used ESI-MS to compare the types of silver hydride/borohydride clusters formed for dpam to those previously reported for dppm,^{16,18} together with their gas-phase chemistry under CID conditions. Clusters of the same stoichiometry which exhibit similar gas-phase chemistry include $[\text{Ag}_3(\text{H})(\text{BH}_4)(\text{L})_3]^+$ and $[\text{Ag}_3(\text{H})(\text{Cl})(\text{L})_3]^+$ (where L = dppm and dpam). In contrast $[\text{Ag}_{10}(\text{H})_8(\text{dpam})_6]^{2+}$ is not observed, while the following clusters with new stoichiometries are observed: $[\text{Ag}_2(\text{BH}_4)(\text{dpam})_2]^+$, $[\text{Ag}_2(\text{BH}_4)(\text{dpam})_3]^+$ and

[Ag₃(BH₄)₂(dpam)₃]⁺. Attempts to crystallize and structurally characterize any of these new clusters via X-ray crystallography have been unsuccessful to date. Work is underway to explore the types of clusters formed upon reaction of copper(I) salts with NaBH₄ and dpam and will be reported in due course.

CONFLICTS OF INTEREST

There are no conflicts to declare.

ACKNOWLEDGEMENTS

We thank the Australian Research Council for financial support (DP150101388, DP180101187 and LE160100015). We thank Dr. Bun Chan (Nagasaki University) for helpful discussions on DFT calculations. HZM thanks the Australian government for a Research Training Program (RTP) scholarship. The DFT calculations were carried out using the HPC facility of The University of Melbourne (punim0255) and at the National Computing Infrastructure. We thank Prof. George Koutsantonis (University of Western Australia) for the gift of a sample of bis(diphenylarsino)methane which provided results for our initial experiments in this work.

ASSOCIATED CONTENT

Electronic Supporting Information (ESI) available: Supplementary spectra, tables, cartesian coordinates of DFT calculated structures.

AUTHOR INFORMATION

Corresponding Author E-mail: rohair@unimelb.edu.au (RAJO)

REFERENCES

- (1) A. J. Jordan, G. Lalic, J. P. Sadighi. Coinage Metal Hydrides: Synthesis, Characterization, and Reactivity. *Chem. Rev.* **2016**, *116*, 8318.
- (2) W. S. Mahoney, D. M. Brestensky, J. M. Stryker. Selective hydride-mediated conjugate reduction of α,β -unsaturated carbonyl compounds using $[(\text{Ph}_3\text{P})\text{CuH}]_6$. *J. Am. Chem. Soc.* **1988**, *110*, 291.
- (3) A. Zavras, G. N. Khairallah, M. Krstić, M. Girod, S. Daly, R. Antoine, P. Maitre, R. J. Mulder, S.-A. Alexander, V. Bonačić-Koutecký, P. Dugourd, R. A. J. O'Hair. Ligand-induced Substrate Steering and Reshaping of $[\text{Ag}_2(\text{H})]^+$ Scaffold for Selective CO_2 Extrusion from Formic Acid. *Nat. Commun.* **2016**, *7*, 11746.
- (4) A. Zavras, J. M. White, R. A. J. O'Hair. An unusual co-crystal $[(\mu_2\text{-dcpm})\text{Ag}_2(\mu_2\text{-O}_2\text{CH})(\eta_2\text{-NO}_3)]_2 \cdot [(\mu_2\text{-dcpm})_2\text{Ag}_4(\mu_2\text{-NO}_3)_4]$ and its connection to the selective decarboxylation of formic acid in the gas phase. *Dalton Trans.* **2016**, *45*, 19408.
- (5) A. Zavras, M. Krstić, P. Dugourd, V. Bonačić-Koutecký, R. A. J. O'Hair. Selectivity Effects in Bimetallic Catalysis: Role of the Metal Sites in the Decomposition of Formic Acid into H_2 and CO_2 by the Coinage Metal Binuclear Complexes $[\text{dppmMM}'(\text{H})]^+$. *ChemCatChem* **2017**, *9*, 1298.
- (6) M. Krstić, Q. Jin, G. N. Khairallah, R. A. J. O'Hair, V. Bonačić-Koutecký. How to Translate the $[\text{LCu}_2(\text{H})]^+$ Catalysed Selective Decomposition of Formic Acid into H_2 and CO_2 from the Gas-phase into a Zeolite. *ChemCatChem* **2018**, *10*, 1173.

- (7) M. F. Bertino, Z.-M. Sun, R. Zhang, L.-S. Wang. Facile Syntheses of Monodisperse Ultra-Small Au Clusters. *J. Phys. Chem. B* **2006**, *110*, 21416.
- (8) D. E. Bergeron, J. W. Hudgens. Ligand Dissociation and Core Fission from Diphosphine-Protected Gold Clusters. *J. Phys. Chem. C* **2007**, *111*, 8195.
- (9) J. S. Golightly, L. Gao, A. W. Castleman, Jr., D. E. Bergeron, J. W. Hudgens, R. J. Magyar, C. A. Gonzalez. Impact of Swapping Ethyl for Phenyl Groups on Diphosphine-Protected Undecagold. *J. Phys. Chem. C* **2007**, *111*, 14625.
- (10) D. E. Bergeron, O. Coskuner, J. W. Hudgens, C. A. Gonzalez. Ligand Exchange Reactions in the Formation of Diphosphine-Protected Gold Clusters. *J. Phys. Chem. C* **2008**, *112*, 12808.
- (11) J. M. Pettibone, J. W. Hudgens. Synthetic Approach for Tunable, Size-Selective Formation of Monodisperse, Diphosphine-Protected Gold Nanoclusters. *J. Phys. Chem. Lett.* **2010**, *1*, 2536.
- (12) A. Olivares, J. Laskin, G. E. Johnson. Investigating the Synthesis of Ligated Metal Clusters in Solution Using a Flow Reactor and Electrospray Ionization Mass Spectrometry. *J. Phys. Chem. A* **2014**, *118*, 8464.
- (13) J. W. Hudgens, J. M. Pettibone, T. P. Senftle, R. N. Bratton. Reaction Mechanism Governing Formation of 1,3-Bis(diphenylphosphino)propane-Protected Gold Nanoclusters. *Inorg. Chem.* **2011**, *50*, 10178.
- (14) J. M. Pettibone, J. W. Hudgens. Reaction network governing diphosphine-protected gold nanocluster formation from nascent cationic platforms. *Phys. Chem. Chem. Phys.* **2012**, *14*, 4142.

- (15) J. M. Pettibone, J. W. Hudgens. Predictive Gold Nanocluster Formation Controlled by Metal-Ligand Complexes. *Small* **2012**, *8*, 715.
- (16) A. Zavras, G. N. Khairallah, T. U. Connell, J. M. White, A. J. Edwards, P. S. Donnelly, R. A. J. O'Hair. Synthesis, Structure and Gas-Phase Reactivity of a Silver Hydride Complex $[\text{Ag}_3((\text{Ph}_2\text{P})_2\text{CH}_2)_3(\mu_3\text{-H})\text{Cl}]\text{BF}_4$. *Angew. Chem. Int. Ed.* **2013**, *52*, 8391.
- (17) A. Zavras, G. N. Khairallah, T. U. Connell, J. M. White, A. J. Edwards, R. J. Mulder, P. S. Donnelly, R. A. J. O'Hair. Synthesis, Structural Characterization and Gas-Phase Unimolecular Reactivity of the Silver Hydride Nanocluster $[\text{Ag}_3((\text{PPh}_2)_2\text{CH}_2)_3(\mu_3\text{-H})](\text{BF}_4)_2$. *Inorg. Chem.* **2014**, *53*, 7429.
- (18) A. Zavras, A. Ariaferd, G. N. Khairallah, J. M. White, R. J. Mulder, A. J. Canty, R. A. J. O'Hair. Synthesis, Structure and Gas-Phase Reactivity of the Mixed Silver Hydride Borohydride Nanocluster $[\text{Ag}_3(\mu_3\text{-H})(\mu_3\text{-BH}_4)\text{L}^{\text{Ph}}_3]\text{BF}_4$ ($\text{L}^{\text{Ph}} = \text{bis}(\text{diphenylphosphino})\text{methane}$). *Nanoscale* **2015**, *7*, 18129.
- (19) J. Li, J. M. White, R. J. Mulder, G. E. Reid, P. S. Donnelly, R. A. J. O'Hair. Synthesis, Structural Characterization and Gas-Phase Unimolecular Reactivity of Bis(diphenylphosphino)amino Copper Hydride Nanoclusters $[\text{Cu}_3(\text{X})(\mu_3\text{-H})((\text{PPh}_2)_2\text{NH})_3](\text{BF}_4)$, where $\text{X} = \mu_2\text{-Cl}$ and $\mu_3\text{-BH}_4$. *Inorg. Chem.* **2016**, *55*, 9858.
- (20) H. Z. Ma, J. Li, A. J. Canty, R. A. J. O'Hair. Cluster transformation of $[\text{Cu}_3(\mu_3\text{-H})(\mu_3\text{-BH}_4)((\text{PPh}_2)_2\text{NH})_3](\text{BF}_4)$ to $[\text{Cu}_3(\mu_3\text{-H})(\mu_2,\mu_1\text{-S}_2\text{CH})((\text{PPh}_2)_2\text{NH})_3](\text{BF}_4)$ via reaction with CS_2 . X-ray structural characterisation and reactivity of cationic clusters explored by multistage mass spectrometry and computational studies. *Dalton Trans.* **2017**, *46*, 14995.

- (21) H. Z. Ma, J. M. White, R. J. Mulder, G. E. Reid, A. J. Canty, R. A. J. O'Hair. Synthesis, Structure, and Condensed-Phase Reactivity of $[\text{Ag}_3(\mu_3\text{-H})(\mu_3\text{-BH}_4)\text{L}^{\text{Ph}}_3](\text{BF}_4)$ (L^{Ph} = bis(diphenylphosphino)amine) with CS_2 . *Dalton Trans.* **2018**, 47, 14713.
- (22) J. Li, H. Z. Ma, G. E. Reid, A. J. Edwards, Y. Hong, J. M. White, R. J. Mulder, R. A. J. O'Hair. Synthesis and X-ray Crystallographic Characterisation of Frustum-Shaped Ligated $[\text{Cu}_{18}\text{H}_{16}(\text{DPPE})]^{2+}$ and $[\text{Cu}_{16}\text{H}_{14}(\text{DPPA})_6]^{2+}$ Nanoclusters and Studies on their H_2 Evolution Reactions *Chem. Eur. J.* **2018**, 24, 2070.
- (23) H. Z. Ma, A. I. McKay, A. Mravak, M. S. Scholz, J. M. White, R. J. Mulder, E. J. Bieske, V. Bonačić-Koutecký, R. A. J. O'Hair. Structural Characterization and Gas-phase Studies of the $[\text{Ag}_{10}\text{H}_8\text{L}_6]^{2+}$ Nanocluster Dication. *Nanoscale*, **2019**, 11, 22880.
- (24) S. Daly, M. Krstić, A. Giuliani, R. Antoine, L. Nahon, A. Zavras, G. N. Khairallah, V. Bonačić-Koutecký, P. Dugourd, R. A. J. O'Hair. Gas-phase VUV Photoionization and Photofragmentation of the Silver Deuteride Nanocluster $[\text{Ag}_{10}\text{D}_8\text{L}_6]^{2+}$ (L = bis(diphenylphosphino)methane). A Joint Experimental and Theoretical Study. *Phys. Chem. Chem. Phys.* **2015**, 17, 25772.
- (25) M. Krstić, A. Zavras, G. N. Khairallah, P. Dugourd, V. Bonačić-Koutecký, R. A. J. O'Hair. ESI/MS Investigation of Routes to the Formation of Silver Hydride Nanocluster Dications $[\text{Ag}_x\text{H}_{x-2}\text{L}_y]^{2+}$ and Gas-phase Unimolecular Chemistry of $[\text{Ag}_{10}\text{H}_8\text{L}_6]^{2+}$. *Int. J. Mass Spectrom.* **2017**, 413, 97.
- (26) A. J. Clark, A. Zavras, G. N. Khairallah, R. A. J. O'Hair. Bis(dimethylphosphino)methane-Ligated Silver Chloride, Cyanide and Hydride Cluster Cations: Synthesis and Gas-Phase Unimolecular Reactivity. *Int. J. Mass Spectrom.* **2015**, 378, 86.

- (27) A. Zavras, A. Mravak, M. Bužančić, J. M. White, V. Bonačić-Koutecký, R. A. J. O'Hair. Structure of the Ligated Ag₆₀ Nanoparticle [$\{Cl@Ag_{12}\}@Ag_{48}(dppm)_{12}$] (where dppm = bis(diphenylphosphino)methane). *Chin. J. Chem. Phys.* **2019**, *32*, 182.
- (28) C. D. Nicola, Effendy, F. Fazaroh, C. Pettinari, B. W. Skelton, N. Somers, A. H. White. Structural characterization of 1:1 adducts of silver(I) (pseudo-) halides (AgX, X=NCO, Cl, Br, I) with Ph₂E(CH₂EPh₂) (E=P, As) ('dp(p/a)m') and 4:3 adducts of copper(I) halide (CuX, X=Cl, Br, I), containing trinuclear cations, of the form [X₂Ag₃(dppm)₃]X and [X₂Cu₃(dppm)₃](CuX₂) and the novel neutral [(OCN)₃Ag₃(dpam)₃]. *Inorg. Chim. Acta* **2005**, *358*, 720.
- (29) J. P. Perdew, K. Burke, M. Ernzerhof. Generalized Gradient Approximation Made Simple. *Phys. Rev. Lett.* **1996**, *77*, 3865.
- (30) J. P. Perdew, K. Burke, M. Ernzerhof. Generalized Gradient Approximation Made Simple. [Phys. Rev. Lett. 77, 3865, (1996)] *Phys. Rev. Lett.* **1997**, *78*, 1396.
- (31) F. Weigend, R. Ahlrichs. Balanced basis sets of split valence, triple zeta valence and quadruple valence quality for H to Rn: Design and assessment of accuracy. *Phys. Chem. Chem. Phys.* **2005**, *7*, 3297.
- (32) F. Weigend, Accurate Coulomb-fitting basis sets for H to Rn. *Phys. Chem. Chem. Phys.* **2006**, *8*, 1057.
- (33) D. Andrae, U. Häußermann, M. Dolg, H. Stoll, H. Preuß. Energy-adjusted ab initio pseudopotentials for the second and third row transition elements. *Theor. Chim. Acta* **1990**, *77*, 123.

- (34) K. A. Peterson, D. Figgen, E. Goll, H. Stoll, M. Dolg. Systematically convergent basis sets with relativistic potentials. II. Small-core pseudopotentials and correlation consistent basis sets for the post-d group 16-18 elements. *J. Chem. Phys.* **2003**, *119*, 11113.
- (35) A. Schäfer, H. Horn, R. Ahlrichs. Fully optimized contracted Gaussian basis sets for atoms Li to Kr. *J. Chem. Phys.* **1992**, *97*, 2571.
- (36) K. Eichkorn, F. Weigend, O. Treutler, R. Ahlrichs. Auxillary basis sets for main row atoms and transition metals and their use to approximate Coulomb potentials. *Theor. Chem. Acc.* **1997**, *97*, 119.
- (37) S. Grimme, J. Antony, S. Ehrlich, H. Krieg. A consistent and accurate ab initio parametrization of density functional dispersion correction (DFT-D) for the 94 elements H-Pu. *J. Chem. Phys.* **2010**, *132*, 154104.
- (38) Gaussian 16, Revision B.01, M. J. Frisch, G. W. Trucks, H. B. Schlegel, G. E. Scuseria, M. A. Robb, J. R. Cheeseman, G. Scalmani, V. Barone, G. A. Petersson, H. Nakatsuji, X. Li, M. Caricato, A. V. Marenich, J. Bloino, B. G. Janesko, R. Gomperts, B. Mennucci, H. P. Hratchian, J. V. Ortiz, A. F. Izmaylov, J. L. Sonnenberg, D. Williams-Young, F. Ding, F. Lipparini, F. Egidi, J. Goings, B. Peng, A. Petrone, T. Henderson, D. Ranasinghe, V. G. Zakrzewski, J. Gao, N. Rega, G. Zheng, W. Liang, M. Hada, M. Ehara, K. Toyota, R. Fukuda, J. Hasegawa, M. Ishida, T. Nakajimi, Y. Honda, O. Kitao, H. Nakai, T. Vreven, K. Throssell, J. A. Montgomery, Jr., J. E. Peralta, F. Ogliaro, M. J. Bearpark, J. J. Heyd, E. N. Brothers, K. N. Kudin, V. N. Staroverov, T. A. Keith, R. Kobayashi, J. Normand, K. Raghavachari, A. P. Rendell, J. C. Burant, S. S. Iyengar, J. Tomasi, M. Cossi, J. M. Millam, M. Klene, C. Adamo, R. Cammi, J. W. Ochterski, R. L.

- Martin, K. Morokuma, O. Farkas, J. B. Foresman, and D. J. Fox, Gaussian, Inc., Wallingford CT, 2016.
- (39) N. Mardirossian, M. Head-Gordon. ω B97M-V: A combinatorially optimized, range-separated hybrid, meta-GGA density functional with VV10 nonlocal correlation. *J. Chem. Phys.* **2016**, *144*, 214110.
- (40) A. Najibi, L. Goerigk. The Nonlocal Kernel in van der Waals Density Functionals as an Additive Correction: An Extensive Analysis with Special Emphasis on the B97M-V and ω B97M-V Approaches. *J. Chem. Theory Comput.* **2018**, *14*, 5725.
- (41) S. Grimme, S. Ehrlich, L. Goerigk. Effect of the damping function in dispersion corrected density functional theory. *J. Comput. Chem.* **2011**, *32*, 1456.
- (42) N. Mardirossian, M. Head-Gordon. Mapping the genome of meta-generalized gradient approximation density functionals: The search for B97M-V. *J. Chem. Phys.* **2015**, *142*, 074111.
- (43) H. S. Yu, X. He, S. L. Li, D. G. Truhlar. MN15: A Kohn-Sham global-hybrid exchange-correlation density functional with broad accuracy for multi-reference and single-reference systems and noncovalent interactions. *Chem. Sci.* **2016**, *7*, 5032.
- (44) H. S. Yu, X. He, S. L. Li, D. G. Truhlar. Correction: MN15: MN15: A Kohn-Sham global-hybrid exchange-correlation density functional with broad accuracy for multi-reference and single-reference systems and noncovalent interactions. *Chem. Sci.* **2016**, *7*, 6278.
- (45) B. Chan, P. M. W. Gill, M. Kimura. Assessment of DFT Methods for Transition Metals with the TMC151 Compilation of Data Sets and Comparison with Accuracies for Main-Group Chemistry. *J. Chem. Theory Comput.* **2020**, *15*, 3610.

- (46) F. Neese. The ORCA program system. *WIREs Comput. Mol. Sci.* **2012**, *2*, 73.
- (47) F. Neese. Software update: the ORCA program system, version 4.0. *WIREs Comput. Mol. Sci.* **2018**, *8*, e1327.
- (48) F. Neese. ORCA, versions 4.2.0. MPI für Kohleforschung: Mülheim a. d. Ruhr, Germany, 2019.
- (49) P. K. Chattaraj, B. Gómez, E. Chamorro, J. Santos, P. Fuentealba. Scrutiny of the HSAB Principle in Some Representative Acid–Base Reactions. *J. Phys. Chem. A* **2001**, *105*, 8815.
- (50) L. S. Bonnington, R. K. Coll, E. J. Gray, J. I. Flett, W. Henderson. Electrospray mass spectrometric investigation of the relative ligand properties of EPh₃ ligands (E=P, As, Sb or Bi) towards Ag⁺ and Cu⁺. *Inorg. Chim. Acta* **1999**, *290*, 213.
- (51) A. Ghisolfi, C. Fliedel, P. de Fremont, P. Braunstein. Mono- and polynuclear Ag(I) complexes of N-functionalized bis(diphenylphosphino)amine DPPA-type ligands: synthesis, solid-state structures and reactivity. *Dalton Trans.* **2017**, *46*, 5571.
- (52) N. V. Belkova, I. E. Golub, E. I. Gutsul, K. A. Lyssenko, A. S. Peregudov, V. D. Makhaev, O. A. Filippov, L. M. Epstein, A. Rossin, M. Peruzzini, E. S. Shubina. Binuclear Copper(I) Borohydride Complex Containing Bridging Bis(diphenylphosphino)Methane Ligands: Polymorphic Structures of [(μ_2 -dppm)₂Cu₂(η^2 -BH₄)₂] Dichloromethane Solvate. *Crystals* **2017**, *7*, 2073.
- (53) N. Gorgas, B. Stöger, L. F. Veiros, K. Kirchner. Access to Fe^{II} (Bis(σ -B-H) Aminoborane Complexes through Protonation of a Borohydride Complex and Dehydrogenation of Amine-Boranes. *Angew. Chem. Int. Ed.* **2019**, *58*, 13874.

- (54) B. E. Green, C. H. L. Kennard, G. Smith, B. D. James, P. C. Healy, A. H. White. Crystal and molecular structure of μ -tetrahydroborato-bis[bis(triphenylphosphine)copper(I)] perchlorate. *Inorg. Chim. Acta* **1984**, *81*, 147.
- (55) S. V. Safronov, E. I. Gutsul, I. E. Golub, F. M. Dolgushin, Y. V. Nelubina, O. A. Filippov, L. M. Epstein, A. S. Peregudov, N. V. Belkova, E. S. Shubina. Synthesis, structural properties and reactivity of ruthenocene-based pincer Pd(II) tetrahydroborate. *Dalton Trans.* **2019**, *48*, 12720.
- (56) V. D. Makhaev, Structural and dynamic properties of tetrahydroborate complexes. *Russ. Chem. Rev.* **2000**, *69*, 727.
- (57) M. Besora, A. Lledós, Coordination Modes and Hydride Exchange Dynamics in Transition Metal Tetrahydroborate Complexes. *Struct. Bond.* **2008**, *130*, 149.
- (58) J. T. Mague, "Short-Bite" Ligands in Cluster Synthesis. *J. Cluster Sci.* **1995**, *6*, 217.

Scheme Captions:

Scheme 1: Bis(phosphine) stabilized silver and copper nanoclusters characterized by X-ray crystallography via a “mass spectrometry directed synthesis” approach (dppm = bis(diphenylphosphine) = $(\text{Ph}_2\text{P})_2\text{CH}_2$; dppe = bis(diphenylphosphino)ethylene = $(\text{Ph}_2\text{P})_2(\text{CH}_2)_2$; dppe = bis(diphenylphosphino)ethylene = $(\text{Ph}_2\text{P})_2(\text{CH}_2)_2$; dppe = bis(diphenylphosphino)ethylene = $(\text{Ph}_2\text{P})_2(\text{CH}_2)_2$; dppe = bis(diphenylphosphino)ethylene = $(\text{Ph}_2\text{P})_2(\text{CH}_2)_2$).

Figure Captions:

Figure 1: Full ion trap ESI-MS spectra of: (A) reaction mixture of (1:1) AgBF_4 : dpam (L) pre-addition of NaBH_4 in CH_3CN showing the formation of $[\text{Ag}(\text{CH}_3\text{CN})(\text{L})]^+$ (m/z 620), $[\text{Ag}(\text{L})_2]^+$ (m/z 1053), $[\text{Ag}_2(\text{Cl})(\text{L})_2]^+$ (m/z 1195) and $[\text{Ag}_3(\text{Cl})_2(\text{L})_3]^+$ (m/z 1810), and; (B) post-addition of 10 eq. NaBH_4 after 15 min. mixing in CH_3CN showing the formation of the cluster ions

$[\text{Ag}_2(\text{BH}_4)(\text{L})_2]^+$ (m/z 1175), $[\text{Ag}_2(\text{BH}_4)(\text{L})_3]^+$ (m/z 1646), $[\text{Ag}_3(\text{H})(\text{BH}_4)(\text{L})_3]^+$ (m/z 1756) and $[\text{Ag}_3(\text{BH}_4)_2(\text{L})_3]^+$ (m/z 1768). m/z values shown are of the most intense peak in the isotopic envelope of the cluster. See Experimental for more information on sample preparation.

Figure 2: CID MSⁿ spectra of most abundant isotopologue of $[\text{Ag}_2(\text{BH}_4)(\text{L})_2]^+$ (m/z 1174.8795) (L = dpam) obtained using a Q value of 0.25 and an activation time of 10 ms with the given Normalized Collision Energy (NCE) for the following species; (A) MS² on $[\text{Ag}_2(\text{BH}_4)(\text{L})_2]^+$ (NCE = 24%) and; (B) MS³ on $[\text{Ag}_2(\text{H})(\text{L})_2]^+$ (m/z 1160.8470) (NCE = 22%). (*) indicates mass-selected precursor ion.

Figure 3: CID MSⁿ spectra of mono-isotopic ion of $[\text{Ag}_2(\text{BH}_4)(\text{L})_3]^+$ (m/z 1643.8990) (L = dpam) obtained using a Q value of 0.25 and an activation time of 10 ms with the given Normalized Collision Energy (NCE) for the following species; (A) MS² on $[\text{Ag}_2(\text{BH}_4)(\text{L})_3]^+$ (NCE = 24%) and; (B) MS³ on $[\text{Ag}_2(\text{BH}_4)(\text{L})_2]^+$ (m/z 1171.8839) (NCE = 19%). (*) indicates mass-selected precursor ion.

Figure 4: CID MSⁿ spectra of most abundant isotopologue of $[\text{Ag}_3(\text{H})(\text{BH}_4)(\text{L})_3]^+$ (m/z 1754.8080) (L = dpam) obtained using a Q value of 0.25 and an activation time of 10 ms with the given Normalized Collision Energies (NCE); (A) MS² on $[\text{Ag}_3(\text{H})(\text{BH}_4)(\text{L})_3]^+$ (NCE = 30%) and; (B) MS³ on $[\text{Ag}_3(\text{H})(\text{BH}_4)(\text{L})_2]^+$ (m/z 1282.7934) (NCE = 24%). (*) indicates mass-selected precursor ion.

Figure 5: CID MSⁿ spectra of most abundant isotopologue of $[\text{Ag}_3(\text{BH}_4)_2(\text{L})_3]^+$ (m/z 1770.8419) (L = dpam) obtained using a Q value of 0.25 and an activation time of 10 ms with the given Normalized Collision Energies (NCE); (A) MS² on $[\text{Ag}_3(\text{BH}_4)_2(\text{L})_3]^+$ (NCE = 28%) and; (B) MS³

on $[\text{Ag}_3(\text{H})(\text{BH}_4)(\text{L})_2]^+$ (m/z 1284.7932) (NCE = 23%). (*) indicates mass-selected precursor ion, (#) indicates an impurity.

Figure 6: Gas-phase models of parent clusters illustrating the Ag_3 core framework and key anion binding interactions; (A) $[\text{Ag}_2(\text{BH}_4)(\text{dpam})_2]^+$ (Isomer 1); (B) $[\text{Ag}_2(\text{BH}_4)(\text{dpam})_2]^+$ (Isomer 2); (C) $[\text{Ag}_3(\text{H})(\text{BH}_4)(\text{dpam})_3]^+$; (D) $[\text{Ag}_3(\text{BH}_4)_2(\text{dpam})_3]^+$; (E) $[\text{Ag}_3(\text{H})(\text{Cl})(\text{dpam})_3]^+$ and; (F) $[\text{Ag}_3(\text{I})(\text{BH}_4)(\text{dpam})_3]^+$. Only the *ipso* carbon atoms of the phenyl rings are shown. DFT structures visualized using Chemcraft – graphical program for visualization of quantum chemical calculations.

Figure 7: Energy diagram for the unimolecular reactivity (BH_3 loss vs. ligand dissociation) of $[\text{Ag}_2(\text{BH}_4)(\text{L})_2]^+$ ($\text{L} = \text{dpam}$) obtained from $\omega\text{B97M-D3BJ/def2-TZVP//RI-PBE/RECP-def2-SVP}$ calculations. Energies ΔG (ΔH) in kcal mol^{-1} relative to parent ion.

Table Captions:

Table 1: Comparison of selected bond lengths (\AA) in the $[\text{Ag}_3(\text{X})_2(\text{L})_3]^+$ framework, where $\text{X} = \text{H}, \text{BH}_4^-$ or Cl^- .

Table 2: Energetics of ligand loss vs. BH_3 loss in the BH_4^- cluster ions $[\text{Ag}_2(\text{BH}_4)(\text{dpam})_2]^+$, $[\text{Ag}_3(\text{H})(\text{BH}_4)(\text{dpam})_3]^+$, $[\text{Ag}_3(\text{BH}_4)_2(\text{dpam})_3]^+$ and $[\text{Ag}_3(\text{I})(\text{BH}_4)(\text{dpam})_3]^+$ obtained from $\omega\text{B97M-D3BJ/def2-TZVP//RI-PBE/RECP-def2-SVP}$ calculations. Energies ΔG (ΔH) in kcal mol^{-1} relative to parent ion.